ELSEVIER

Cement & Concrete Composites 26 (2004) 57–73

Cement & Concrete Composites

www.elsevier.com/locate/cemconcomp

Finite element modeling of coupled heat transfer, moisture transport and carbonation processes in concrete structures

O. Burkan Isgor [a], A. Ghani Razaqpur [b,*]

[a] Gorex Consulting, 1403-100 Boteler Street, Ottawa, ON, Canada K1N 8Y1

[b] Department of Civil and Environmental Engineering, Carleton University, 1125 Colonel By Drive, Ottawa, Ont., Canada K1N 8Y1

Accepted 29 October 2002

Abstract

Carbonation is one of the many reasons of reinforcement corrosion in concrete structures. Due to the coupling effects of moisture, heat and carbon dioxide transport in concrete, the modeling of this problem is a rather challenging task. A nonlinear finite element approach is adopted here for tracing the spatial and temporal advancement of the carbonation front in concrete structures with and without cracks. A two-dimensional Windows-based finite element computer program, called CONDUR, is developed and the results obtained from the program are compared with available experimental data. The program is designed to be flexible and comprehensive in its scope.

Keywords: Carbonation; Concrete; Corrosion of reinforcement; Durability; Heat transfer; Moisture transfer; Finite element modeling

1. Introduction

The deterioration of reinforced concrete structures, primarily due to corrosion of steel reinforcement, has become a major concern of infrastructure owners and operators. The deterioration is generally caused by the exposure of the reinforced concrete structures to salts and/or carbonation. In the case of carbonation, chemical reaction between carbon dioxide from the air and the hydration products of cement in concrete causes a reduction in the alkalinity of concrete and consequently in its ability to protect the steel reinforcement from corrosion [1–5]. Therefore, to protect the vast public investment in the concrete infrastructure, research is currently conducted at various institutions to develop new and improved construction materials, rehabilitation and repair technologies, and a better understanding of the physical and chemical mechanisms that lead to deterioration. The improved knowledge will enable designers not only to properly rehabilitate and maintain the current stock of concrete structures, but also to improve the durability of future structures by giving, in the design stage, proper consideration to the environment and conditions within which they operate. To prevent premature deterioration of concrete structures, design and maintenance guidelines have been issued by a number of organizations including the American Concrete Institute [6] and the Canadian Standards Association [7]. However, these guidelines do not give designers the ability to quantitatively assess the combined effect of a number of parameters in a detailed fashion.

The work described in the present paper will enable designers to carry out detailed simulations in order to arrive at a more realistic expectation of the long-term performance of structures, subjected to variable exposure conditions in severe environments, and is a part of a larger scale research study which focuses on the modeling of the corrosion of reinforcement in concrete structures due to coupled chloride exposure and carbonation under variable environmental conditions. It is important to state at the outset that the validity of the results of the model, similar to any other numerical model, will depend on the accuracy of the input data used and is circumscribed by the underlying assumptions

* Corresponding author. Tel.: +1-613-520-2600; fax: +1-613-520-3951.

E-mail address: ghani_razaqpur@carleton.ca (A.G. Razaqpur).

0958-9465/$ - see front matter © 2003 Elsevier Ltd. All rights reserved.
doi:10.1016/S0958-9465(02)00125-7

and limitations of the model. Without losing sight of the preceding caveat, the writers believe that the proposed framework will enable designers to carry out more robust sensitivity analyses and to gauge the significance of variations in the values of certain parameters on the rate of carbonation in concrete structures. In this paper, we focus on the problem of carbonation and its effects on the durability of reinforced concrete structures. Specifically, the diffusion of carbon dioxide into concrete is modeled as a two-dimensional transient problem. The dependence of carbon dioxide diffusion rate on the moisture and the temperature is modeled and the detailed time-dependent reduction in pH due to carbonation is determined. Due to the importance of the moisture content of concrete on the diffusion process of carbon dioxide, the moisture diffusion process is treated as a temperature-dependent phenomenon.

In view of the ability of the finite element method to treat complex boundary and initial conditions, it is applied in the present study. A two-dimensional Windows-based finite element program, called CONDUR, is developed to trace the time, moisture and temperature-dependent diffusion of carbon dioxide in concrete. The program determines the complete distribution of temperature, moisture and CO_2 within the structure at specified times after initial exposure. An attempt is made, albeit in an elementary fashion, to include the effect of carbonation on the microstructure of concrete and on changes in its CO_2 diffusion coefficient. It is the intention of this work to provide researchers and designers alike with a tool to assess the long-term durability of concrete structures subjected to carbonation. It is not the purpose of this study to propose new theoretical models for the phenomena that influence the carbonation process.

2. Mechanism of carbonation damage

To facilitate the discussion with respect to the finite element modeling technique applied in this study, fundamental physics and chemistry of carbonation are presented. The reinforcing steel inside the concrete is generally covered by a passivating layer, basically a form of iron oxide, which acts as a protective coat for steel. Concrete with its high alkalinity serves as a protective medium for the passivating layer and as long as this protection is present around the steel, corrosion does not start [8]. However, the environment in which the structure operates may weaken or even eliminate the passivating layer around the reinforcement; for instance, CO_2 has the potential to dissolve in concrete pore water and to react with the hydration products, causing a reduction in pH from 13 or 12 to levels below 9. At low pH, concrete loses its protective nature, thereafter, when the embedded steel is exposed to oxygen and ion-bearing solution, the corrosion of the reinforcement commences.

Another important consequence of carbonation is a possible change in the transport properties of concrete induced by volume and pore structure changes. In certain cases the permeability of carbonated concrete may increase, as in the case of concrete made with blended cements such as blast furnace slag (BFS) and fly ash concrete; in others, it may decrease as in ordinary Portland cement (OPC) concrete [9]. It has to be noted that the effect of carbonation on the pore structure and the permeability properties of concrete is a complex problem for which a completely satisfactory model is yet to be developed. Nevertheless, the available models are adequate for providing a reasonable explanation for the observed behavior of reinforced concrete structures subjected to carbonation.

3. Carbonation reactions and their effects

Papadakis et al. [10] have provided a thorough review of the fundamental chemistry of carbonation, and presented a detailed theoretical framework for its prediction. In the following, some of the basic relations are recapped in order to provide the physico-chemical framework for the reactions employed in the numerical model.

Carbonation can simply be defined as the reaction of carbon dioxide (CO_2) with calcium hydroxide ($Ca(OH)_2$) in the hardened cement paste, resulting in the production of calcium carbonate ($CaCO_3$). This reaction occurs as follows:

$$Ca(OH)_2(s) \rightarrow Ca^{2+}(aq) + 2OH^-(aq) \tag{1}$$

where the symbols s and aq within the parenthesis signify solid and aqueous states.

Carbon dioxide also dissolves in concrete pore water and forms carbonic acid before reacting with the dissolved $Ca(OH)_2$, viz.

$$\begin{aligned} &H_2O + CO_2(g) \rightarrow HCO_3^-(aq) + H^+(aq) \\ &HCO_3^-(aq) \rightarrow CO_3^{2-}(aq) + H^+(aq) \end{aligned} \tag{2}$$

The following neutralization reaction completes the final stage of carbonation

$$\begin{aligned} &Ca^{2+}(aq) + 2OH^-(aq) + 2H^+(aq) + CO_3^{2-}(aq) \\ &\quad \rightarrow CaCO_3(s) + 2H_2O \end{aligned} \tag{3}$$

Reaction (3) shows that carbonation consumes $Ca(OH)_2$, a product which endows concrete with high pH. The rates of the reactions (1) and (3) play an important role in the carbonation of concrete. The rate of dissolution of $Ca(OH)_2$ in concrete pore water, r_D, and the rate of the neutralization reaction, r_N, i.e. the reaction rate of CO_2

with dissolved $Ca(OH)_2$, are given by Eqs. (4) and (5), respectively [10]

$$r_D = 1.685 \times 10^{-5} \mu f_w k_s a_s [Ca(OH)_2(s)]([OH^-]_{eq} - [OH^-]) \quad (4)$$

$$r_N = HRTk_2[OH^-]_{eq}[CO_2(g)] \quad (5)$$

where r_D is in moles of $Ca(OH)_2$ dissolved per unit volume of concrete per second, f_w is the volume fraction of the aqueous film on the walls of the pores, μ is the porosity of concrete, k_s is the mass diffusion coefficient for the dissolution of $Ca(OH)_2$ (s), which is approximately 5.0×10^{-5} m/s [10], a_s is the pore area per unit concrete volume, $[Ca(OH)_2(s)]$ is the molar concentration of $Ca(OH)_2$ per unit volume of concrete, $[CO_2(g)]$ is the molar concentration of CO_2 per unit volume of pore air and $[OH^-]$ is the molar concentration of OH^- per unit volume of the aqueous phase in the pores. $[OH^-]_{eq}$ is the molar concentration of (OH^-) at equilibrium, which is equal to 43.2 mol/m^3 at 25 °C, H is Henry's constant for the dissolution of CO_2(g) in water and is equal to 34.2 mol/m^3 atm at 25 °C, R is the universal gas constant, T is the absolute temperature, and k_2 is a rate constant for the reaction of CO_2 and OH^- and is equal to 8.3 m^3/mol s.

The carbonation reactions (1)–(3) occur ideally when the relative humidity of the concrete is between 50% and 70% [8,11]. If the humidity is less than 50%, CO_2 ions cannot be dissolved completely due to inadequate water in the pores, while if is larger than 70%, the water inside the pores inhibits the CO_2 diffusion, resulting in very slow rates of carbonation. Between 50% and 70% relative humidity, as indicated earlier, $Ca(OH)_2$ reacts with CO_2 in a neutralization reaction. The amount of $Ca(OH)_2$ in a fully hydrated OPC concrete can easily be determined if the type of cement used and the concrete mix properties are known [8,10]. The $Ca(OH)_2$ content in a fully hydrated OPC paste is around 30% by weight [11]. The final product of the neutralization reaction, $CaCO_3$, has a very low solubility and contributes to the clogging of the pore system, causing a decrease in the fluid and gas permeability of carbonated OPC concrete. Since the $Ca(OH)_2$ content in BFS or fly ash concrete is very low, the C–S–H phase goes into the carbonation reaction. Although this reaction occurs at a much slower rate than the carbonation of $Ca(OH)_2$, the resulting product will cause an increase in the fluid and gas permeability of concrete [9]. It has to be pointed out that the investigation of the blended cement concrete structures (e.g. BFS or fly ash concrete) is not within the scope of this study.

In order to model the carbonation process in OPC concrete structures, it is imperative to determine the amount of CO_2 diffusing into them. Since the CO_2 transport in concrete is a function of temperature and moisture content, it is necessary to consider these processes when dealing with carbonation.

4. Carbon dioxide diffusion in concrete

As stated earlier, the effect of moisture content and temperature on the carbon dioxide diffusion and on the carbonation processes is important. Therefore, determining carbonation in a concrete structure has to start with the determination of the temperature and moisture profiles. Due to the coupling of the thermal and moisture transport phenomena, a non-linear solution scheme is necessary.

As mentioned before, the carbonation process changes the transport properties of the concrete. In OPC concrete, a reduction in the values of the moisture and CO_2 diffusion coefficients; i.e. D_h and D_c, respectively, has been observed due to carbonation. Although modeling of this change is a very complex theoretical problem, practically based on experimental studies, decay functions for D_h and D_c have been suggested. It has to be noted that moisture transport through wetting and drying cycles may also change the pore structure of concrete [12]; however, this change has not been incorporated in the current model.

The relationship between carbonation and reduction in porosity has been studied by Papadakis et al. [10], and for a fully hydrated concrete, is given as:

$$\mu(t) = f_d(t, \varphi)\mu_0 \quad (6)$$

where $\mu(t)$ is the porosity of concrete at time t, $f_d(t, \varphi)$ is a decay function which may be used to determine the changed porosity of concrete due to carbonation, φ is the degree of carbonation, μ_0 is the initial porosity of concrete. A bi-linear decay function, as in Fig. 1, can be used to simulate the effect of carbonation on the diffusion of moisture and CO_2. The parameters a and b in Fig. 1 can be empirically determined based on observed change in porosity of concrete due to carbonation.

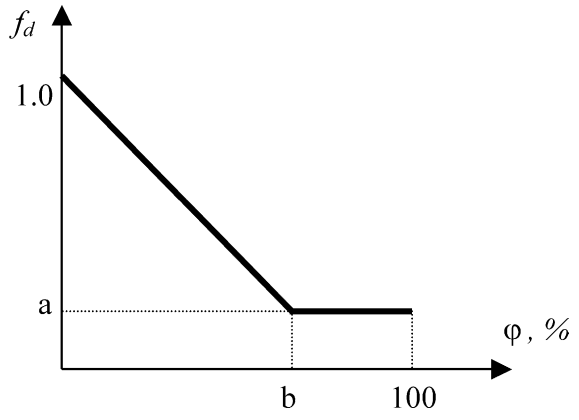

Fig. 1. Decay function as a function of the degree of carbonation.

Alternatively, as indicated by Papadakis et al. [10], change in porosity can be calculated based on the amount of $Ca(OH)_2$ consumed during the carbonation reaction.

Initial porosity of concrete, μ_0, may be either specified or it can be calculated as suggested by Papadakis [10]:

$$\mu_0 = \frac{\frac{w}{c}\frac{\rho_c}{\rho_w}(1-\mu_{air})}{1+\frac{w}{c}\frac{\rho_c}{\rho_w}+\frac{a}{c}\frac{\rho_c}{\rho_a}} + \mu_{air} \tag{7}$$

where for a given concrete, a/c is the aggregate–cement ratio, w/c is the water–cement ratio, μ_{air} is the air content of the concrete, ρ_c, ρ_a and ρ_w are the densities of cement, aggregates and water, respectively.

Finally, although carbonation reactions are exothermic and may affect the heat balance of the system, its contribution to the overall temperature distribution in concrete is rather small, accordingly it may be ignored.

5. Governing transport equations

With the forgoing theoretical and empirical considerations in mind, we now present the governing equations of the important phenomena which affect carbonation. We will deal with two-dimensional transport problems and believe that it is adequate for modeling most practical problems of carbonation. For a two-dimensional problem in an x–y plane, which is the focus of the current study, the governing equations of transport relevant to carbonation are:

5.1. Carbon dioxide transport

The transport of carbon dioxide inside concrete is governed by the following equation:

$$\frac{\partial}{\partial x}\left(D_c\frac{\partial C_c}{\partial x}\right)+\frac{\partial}{\partial y}\left(D_c\frac{\partial C_c}{\partial y}\right)+Q_c=\frac{\partial C_c}{\partial t} \tag{8}$$

where D_c (m^2/s) is the CO_2 diffusion coefficient, C_c (kg/m^3 pore solution) is the CO_2 concentration and Q_c (kg/m^3 s) is a sink term representing the reduction in the CO_2 content of concrete due to carbonation reaction and can be determined using basic principles of chemistry [8,10]. D_c depends on several factors such as temperature, relative humidity, age of concrete, exposure conditions, etc. Different models for the determination of D_c can be found in the literature [10,13,14]; here we apply the following expression proposed by Papadakis et al. [10]:

$$D_c = 1.64\times10^{-6}\mu_p(t)^{1.8}(1-h)^{2.2} \tag{9}$$

where h is the relative humidity, expressed as a fraction, at time t and $\mu_p(t)$ is the porosity of the hardened cement paste given as

$$\mu_p(t) = \mu(t)\left(1+\frac{\frac{a}{c}\frac{\rho_c}{\rho_a}}{1+\frac{w}{c}\frac{\rho_c}{\rho_w}}\right) \tag{10}$$

5.2. Heat transfer

Thermal conduction inside concrete is governed by Fourier's law, which is given by

$$-\frac{\partial}{\partial x}\left(-k\frac{\partial T}{\partial x}\right)-\frac{\partial}{\partial y}\left(-k\frac{\partial T}{\partial y}\right)+Q=\rho c\frac{\partial T}{\partial t} \tag{11}$$

where k is the thermal conductivity of concrete (W/m °C), T is its temperature (°C), ρ is its density (kg/m^3), c is its specific heat (J/kg °C), t is time (s), C_a is the volumetric heat capacity of the air (J/m^3 K), Q is the heat source/sink term.

Although the heat transfer inside the concrete is governed by this equation, the boundary conditions at the concrete surface, such as the presence of wind and solar radiation, affect the temperature profile significantly and must be considered. The net heat flow on a concrete surface can be written as:

$$q_s - q_c - q_r - q_y = 0 \tag{12}$$

where q_s is the total radiation absorbed, q_r is the re-radiation by concrete, q_c is the heat loss by convection and q_y is the heat conducted into the concrete body. Total radiation absorbed by the concrete surface can be calculated from

$$q_s = \alpha I_n \tag{13}$$

where α is the absorbtivity of concrete, which varies between 0.5 and 1.0, and depends on the colour and the texture of the surface [15,16], and I_n is the direct solar radiation intensity [17] which can be approximated [18] using

$$I_n = C_N G_Z e^{(-\tau/\cos\beta)} \tag{14}$$

where C_N is the clearness number, which depends on the location of the structure within the world, and can be obtained from meteorological maps [17]. The quantity β is the solar zenith angle, defined as the angle between the solar radiation and the normal to the horizontal plane at the location of the structure and is a function of the time of the day. Quantities G_z and τ are given by the following trigonometric series

$$\begin{aligned} G_z = {} & 1162.4 + 77.4\cos(C_T) - 3.6\cos(2C_T) - 3.4 \\ & \times \cos(3C_T) + 1.8\sin(C_T) - 0.6\sin(2C_T) \\ & + 0.9\sin(3C_T) \end{aligned} \tag{15}$$

$$\begin{aligned} \tau = {} & 0.1717 - 0.0344\cos(C_T) + 0.0032\cos(2C_T) \\ & + 0.0024\cos(3C_T) - 0.0043\sin(C_T) \\ & - 0.0008\sin(3C_T) \end{aligned} \tag{16}$$

where $C_T = 2\pi n_Y/366$, n_Y is the day of the year. Since some of the direct solar radiation diffuses and dissipates in the atmosphere, I_n has to be modified accordingly. The latter is described in more detail by Clausing [18].

Heat loss through the concrete surface by convection can be calculated by

$$q_c = h_c(T_l - T_{sh}) \tag{17}$$

where T_{sh} is the shade air temperature, T_l is the body surface temperature and h_c is the convection coefficient (W/m^2 °C).

Re-radiation from the concrete surface can be obtained by using Stefan–Boltzman law:

$$q_r = \varepsilon\sigma(T_s^4 - T^{*4}) \tag{18}$$

where ε is the emissivity of gray concrete surface, which is equal to the ratio of emission from gray surface to that from perfect radiator at the same temperature and can be taken as 0.9 for most cases, σ is the Stefan–Boltzman constant (5.669×10^{-8} W/m^2 K^4), T_s is the absolute surface temperature (K) and T^* is the absolute average air temperature (K), which can be approximated as 228 K. Rearranging Eq. (18), we obtain:

$$q_r = h_r(T_1 - T_{sh}) + \varepsilon\sigma(T_{sha}^4 - T^{*4}) \tag{19}$$

where h_r is the radiation heat transfer coefficient (W/m^2 °C) and T_{sha} is the absolute shade temperature (K).

From Fourier's law, the conductive heat transfer through the surface can be written as

$$q_y = -k\left(n_x\frac{\partial T}{\partial x} + n_y\frac{\partial T}{\partial y}\right) \text{ or:} \tag{20}$$

$$q_y = k\left(\frac{\partial T}{\partial n}\right) \tag{21}$$

where n_x and n_y are the direction cosines of the normal n to the surface.

If the convection and radiation heat transfer coefficients are combined ($h_T = h_c + h_r$), and the heat flux equations given in Eqs. (13),(17),(19) and (21) are brought together, the following boundary condition on the concrete surface can be prescribed

$$\alpha I_n - \varepsilon\sigma(T_{sha}^4 - T^{*4}) - h_T(T_1 - T_{sh}) + k\left(\frac{\partial T}{\partial n}\right) = 0 \tag{22}$$

Several researchers have suggested expressions for h_c as a function of average wind speed [19,20]. Since most of these expressions give similar results, the following equation, which is suggested by Priestley and Thurston [19], can be used to evaluate h_c

$$h_c = 13.5 + 3.88v \tag{23}$$

where v is the average wind speed (m/s) and h_c is in W/m^2 °C.

It has to be noted that Eq. (22) requires a nonlinear solution of Eq. (12) due to the T^4 term. However, depending on the time of the day, some simplifications can be made. Since $T_{sha} \cong T^*$ during the daylight, net solar radiation heat flux reduces to αI_n. Similarly since there is no solar radiation during the evening, the radiation heat flux can be calculated as $-\varepsilon\sigma(T_{sha}^4 - T^{*4})$. Further information about the heat transfer modeling in concrete structures can be obtained from Potgieter and Gamble [20].

5.3. Moisture transfer

Moisture flow in concrete can be expressed in two different ways: either in terms of the evaporable or free water, w_e, or in terms of pore relative humidity, h, which is expressed as a fraction. Moisture profile in concrete in terms of pore relative humidity can be determined by solving the following differential equation [21]

$$\frac{\partial}{\partial x}\left(D_h\frac{\partial h}{\partial x}\right) + \frac{\partial}{\partial y}\left(D_h\frac{\partial h}{\partial y}\right) + \frac{\partial h_s}{\partial t} + K\frac{\partial T}{\partial t} + Q_h = \frac{\partial w_e}{\partial h}\frac{\partial h}{\partial t} \tag{24}$$

where $\partial h_s/\partial t$ is the pore relative humidity due to self-desiccation, K is the hygrothremal coefficient (1/°C), which determines the change in humidity due to one degree change in temperature, T, at a constant water content, w_e, Q_h represents the water generated by the carbonation reaction, $\partial T/\partial t$ is the variation of temperature over time, $\partial w_e/\partial h$ is the moisture capacity [22] and $\partial h/\partial t$ is the change in pore water content with time.

In normal strength concrete, the decrease in pore water content, h, due to self-dessication is very small and can be omitted for practical purposes. This assumption has been shown to be true even when the hydration process is not yet complete [21]. For high strength concrete, due to low water–cement ratio of the concrete mix, self-dessication becomes significantly high and has to be taken into account. Since this study is limited to normal strength concrete, the $\partial h_s/\partial t$ term can be set equal to zero. For practical purposes, the effect of heat on moisture transport will be incorporated empirically into the moisture transport coefficient, D_h, and hence the term $\partial T/\partial t$ can also be set to zero. With these assumptions, Eq. (24) can be re-written as

$$\frac{\partial}{\partial x}\left(D_h\frac{\partial h}{\partial x}\right) + \frac{\partial}{\partial y}\left(D_h\frac{\partial h}{\partial y}\right) + Q_h = \frac{\partial w_e}{\partial h}\frac{\partial h}{\partial t} \tag{25}$$

Although empirical expressions have been suggested for Q_h [15], time-dependent nonlinear finite element solution of the governing equation given by Eq. (18) allows one to utilize the basic principles of chemistry to determine these values at each time increment of the iterative solution as long as the amount of CO_2 transported into the concrete and the amount of $Ca(OH)_2$ in the hydrated cement paste are known. The calculated Q_h value can be modeled as a source term in the finite element formulation and Eq. (25) can be solved by using a non-linear solution scheme.

The moisture capacity, $\partial w_e/\partial h$ in Eq. (25) represents the relationship between the evaporable water and pore water contents and can be determined by using one of

the available adsorption isotherms such as Langmuir isotherm, Brunauer, Emmett and Teller (BET) isotherm or FHH isotherm [21]. Using the Brunauer, Skalny and Bodor (BSB) model [21], also known as three-parameter BET isotherm, w_e, can be written as

$$w_e = \frac{Ck_m V_m h}{(1-k_m h)[1+(C-1)k_m h]} \tag{26}$$

where w_e is expressed in terms of grams of water per gram of cementitious material. V_m, which is the amount of vapour required for monolayer (monolayer capacity), and parameters C and k_m can be calculated as follows:

$$C = e^{(855/T)} \tag{27}$$

$$k_m = \frac{\left(1-\frac{1}{n}\right)C-1}{C-1} \tag{28}$$

$$V_m = \left(0.068 - \frac{0.22}{t_e}\right)\left(0.85 + 0.45\frac{w}{c}\right) \tag{29}$$

wherein for (w/c $<$ 0.3): $n = 0.99\left(2.5+\frac{15}{t_e}\right)$

while for (w/c $\geqslant$ 0.6): $n = 1.65\left(2.5+\frac{15}{t_e}\right)$

On the other hand, for (0.3 $<$ w/c $<$ 0.6):

if ($t_e > 5$ days) $n = \left(2.5+\frac{15}{t_e}\right)(0.33+2.2\text{w/c})$

if ($t_e \leqslant 5$ days): $n = 5.5(0.33+2.2\text{w/c})$ where t_e is the equivalent hydration age in days and w/c is the water cement ratio.

The moisture transport coefficient, D_h, depends on several factors such as temperature, existing relative humidity, age of the concrete, exposure condition and duration. Although several researchers [15,23] have

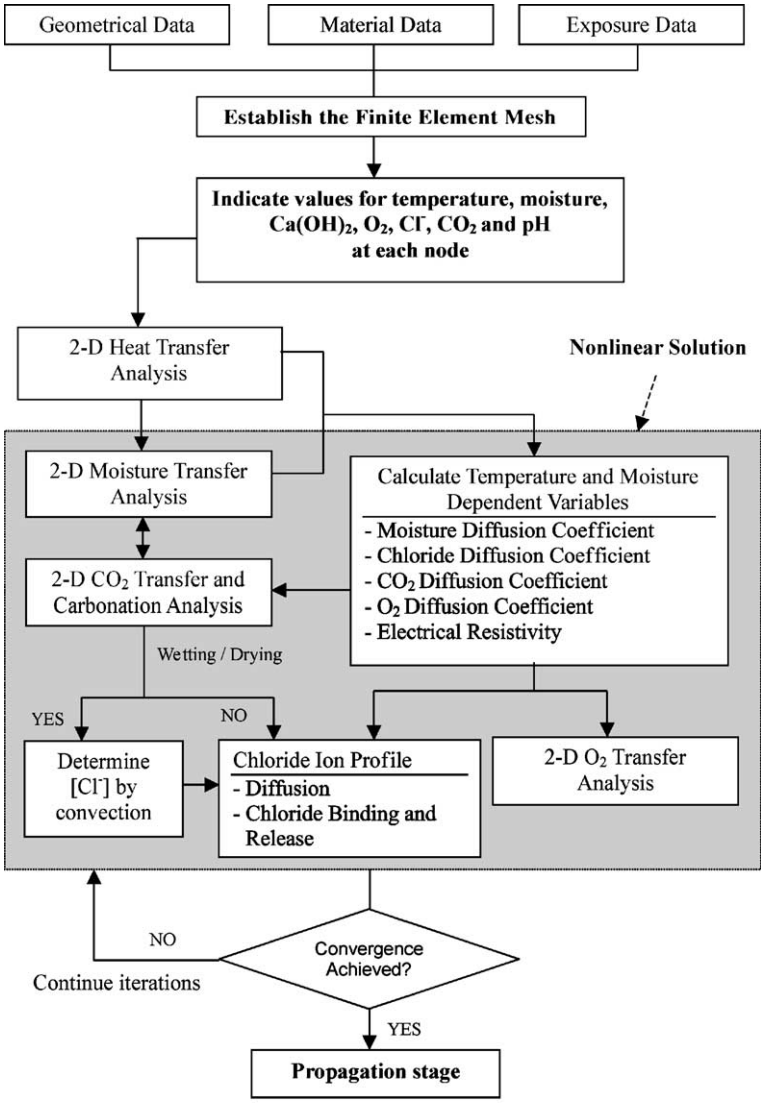

Note: This paper only describes the carbonation related procedures. For details of other processes refer to Isgor (2001).

Fig. 2. Nonlinear solution scheme for the proposed model.

proposed models for the determination of this coefficient, due to the complexity of the problem, further studies on the topic are still in progress. Since it is not our intention to develop a model for D_h, one of the existing models will be utilized in this study. Further information about the material models for moisture transfer in concrete structures can be obtained from Martín-Pérez [21].

6. Proposed model

The proposed finite element model for coupled heat transfer, moisture transport and carbonation process in concrete structures is part of a larger scale research study which mainly focuses on the modeling of the chloride and carbonation induced reinforcement corrosion. With reference to the flowcharts in Figs. 2–5, the proposed model [24] begins with the definition of geometry, material properties, exposure conditions, and CO_2 and $Ca(OH)_2$ initial concentrations. Using the prescribed boundary and initial conditions, thermal and moisture transport analyses are performed using Eqs. (11) and (25), respectively, to determine the temperature and moisture distribution within the structure. Although the coefficient of thermal conduction, k, and specific heat, c, depend on the moisture content of the medium, the effect is not significant for the temperature range one

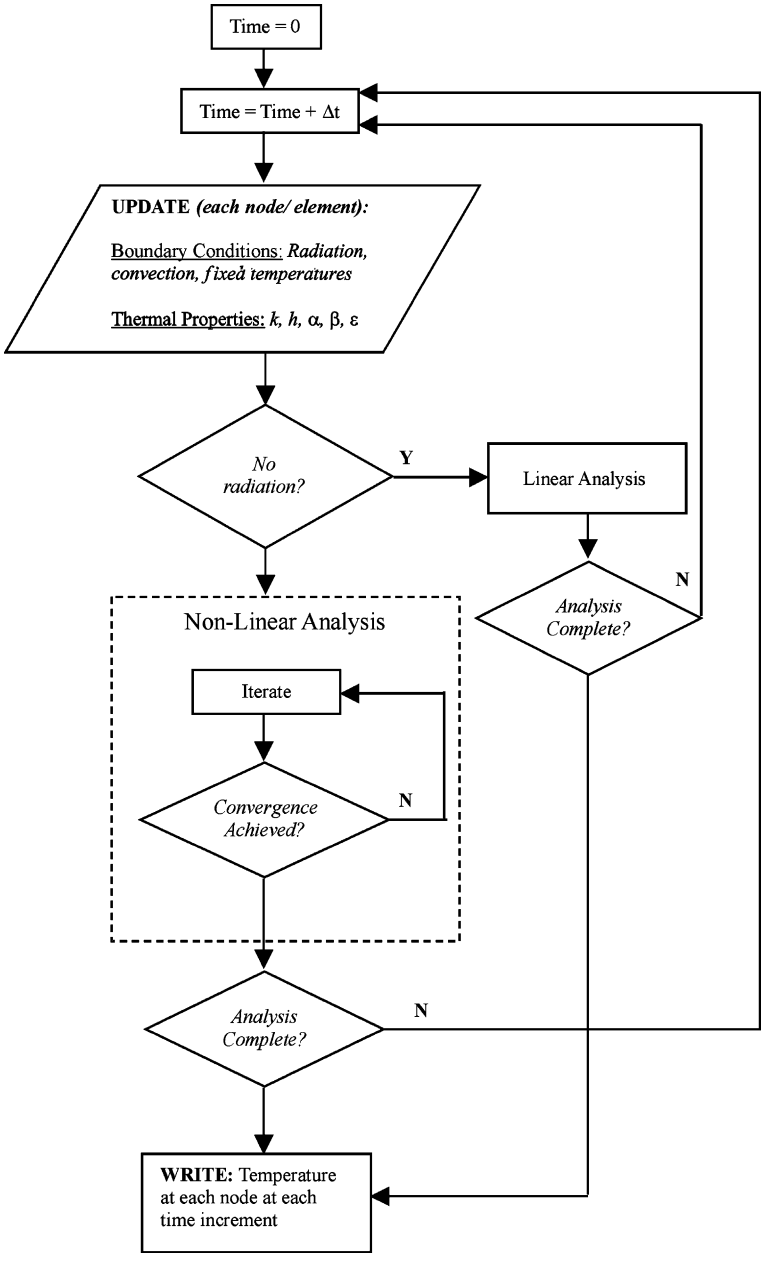

Fig. 3. Flowchart of the heat transfer analysis.

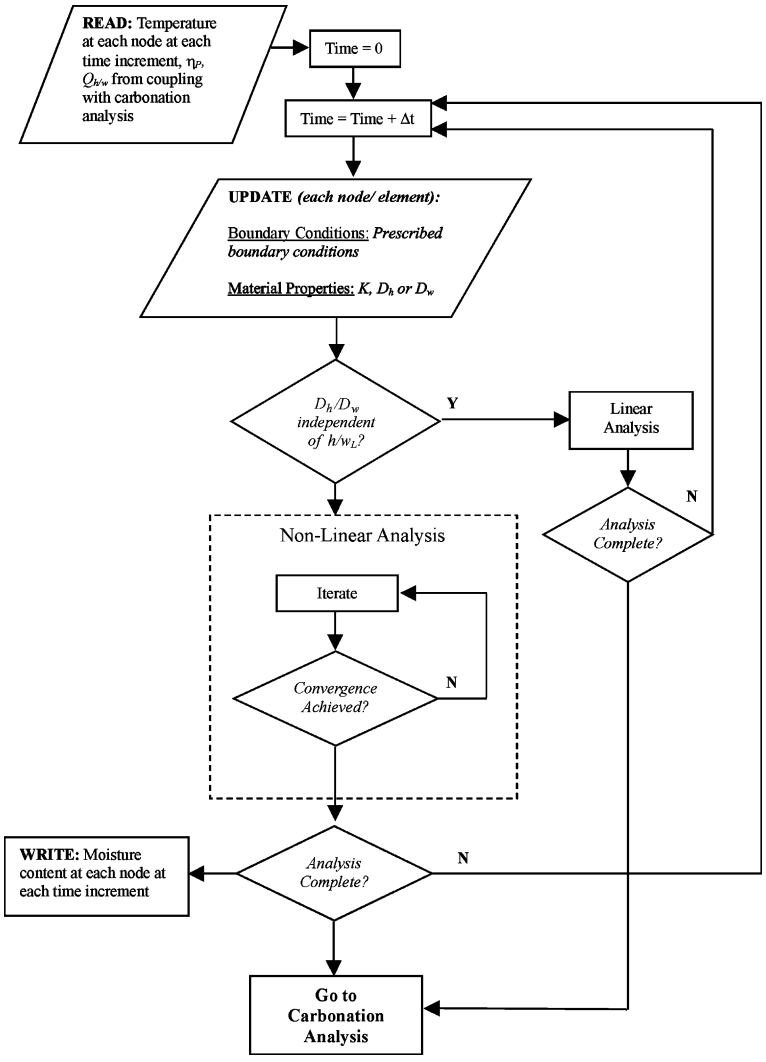

Fig. 4. Flowchart of the moisture transfer analysis.

normally encounters in concrete structures; therefore, they are assumed to be independent of the moisture content. In addition, if there is no radiation in the system and there is no temperature-dependent heat sink or source term, the solution of the heat transfer equation follows a linear solution algorithm; otherwise a nonlinear analysis is used.

As stated previously, since carbonation produces water, which affects the moisture content of concrete, the moisture transfer analysis is coupled with the CO_2 transfer analysis (i.e. carbonation). However, it is a one-way coupling in that the water produced by the carbonation reaction is introduced as a source term, i.e. Q_c in Eq. (25), and its quantity is determined by the rate of carbonation reaction according to Eqs. (4) and (5). Considering the flowcharts in Figs. 4 and 5, the moisture–carbonation coupled analysis is performed in the following manner. First, moisture transfer analysis is performed over the full time domain in increments of time Δt_i. For each Δt_i, the moisture profile is determined and stored in a vector. After the completion of the moisture analysis over the full time domain $t = \sum \Delta t_i$, the carbonation analysis is commenced using the same time increments as in the moisture analysis. The moisture profile corresponding to Δt_i is retrieved and used in the carbonation analysis. During this process, for each time step, the water generated during carbonation, Q_{ci}, is stored in a vector, and the analysis is continued until the end of the full time domain. Upon completion of the carbonation analysis, the moisture analysis is revised and the initial moisture content for each time increment is adjusted by including Q_{ci} as a source term. Hence, the entire moisture analysis is re-performed, followed by a new carbonation analysis. This process is continued until convergence is achieved in terms of the carbonation water production. Once minimal change in the carbonation water content, i.e. ΔQ_{ci}, is reached, the analysis is terminated. The convergence criterion is defined by the user. We recognize that from the numerical analysis point of view, it might be better to perform

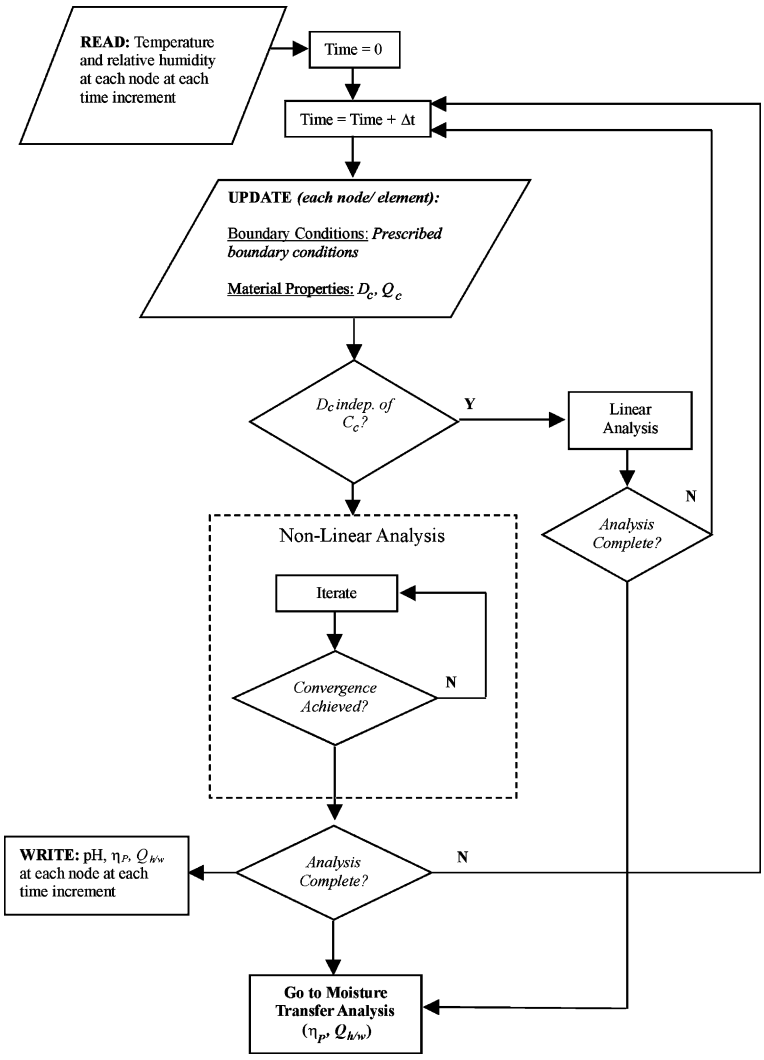

Fig. 5. Flowchart of the CO_2 transfer analysis.

carbonation analysis immediately after the moisture analysis for each time increment and check the convergence of the solution within that increment. However, due to practical consideration, we selected the method described earlier.

Another important consequence of the carbonation process is its affect on the porosity of the concrete. The change in the porosity is assumed to affect the moisture and CO_2 and is modeled by using a bilinear decay function. It has to be noted that the change in the pH of the pore solution is monitored and recorded at each time step since it will be used as a criterion for the chloride release process and in the propagation stage of the model. According to Papadakis et al. [10] the pH of carbonated concrete can be written as

$$\mathrm{pH} = 14 + \log(2 \times 10^3)[\mathrm{Ca(OH)_2}]_{(\mathrm{aq})} \tag{30}$$

Next, the CO_2 diffusion coefficient, D_c, is determined at selected locations in the structure using Eq. (9) in conjunction with the temperature and moisture profiles determined earlier. With D_c known, the CO_2 transport in concrete and its concentration distribution are determined by solving Eq. (8). This is followed by finding the rates of dissolution of $Ca(OH)_2$ and the neutralization reaction according to Eqs. (4) and (5), respectively. From these reactions, the current concentration of CO_2 and $Ca(OH)_2$, and the porosity of concrete, using Eq. (6), are established. This process is continued by performing the analysis over prescribed time interval or until the available $Ca(OH)_2$ has been exhausted. This model is implemented in a nonlinear time-dependent finite element formulation as described next.

7. Finite element implementation

The model presented in the previous section involves several field problems such as heat, moisture and CO_2 transport, each of which can be represented by a quasi-harmonic equation of the form

$$\frac{\partial}{\partial x}\left(k_x\frac{\partial\phi}{\partial x}\right)+\frac{\partial}{\partial y}\left(k_y\frac{\partial\phi}{\partial y}\right)+Q=\rho c\frac{\partial\phi}{\partial t} \tag{31}$$

In the case of heat transfer, the potential, ϕ, in Eq. (31) represents the temperature, T; and k_x and k_y are the thermal conductivities in x and y directions, respectively. In moisture transfer, the potential, ϕ, becomes the relative humidity, h; and k_x, and k_y are the moisture diffusion coefficients, D_{hx} and D_{hy}, respectively. Similarly, in the case of CO_2 diffusion, the potential represents the concentration of CO_2 and k_x and k_y are the diffusion coefficients in the x and y, respectively. The term Q represents the internal generation or consumption of the species or quantity of interest, ρ and c are pertinent material properties. In the case of heat transfer analysis ρ is the density of the medium and c is its specific heat.

Following Logan [25], the functional corresponding to Eq. (31) may be written as π_h

$$\begin{aligned}\pi_h=\frac{1}{2}\int_V\int\int\left[k_x\left(\frac{\partial\phi}{\partial x}\right)^2k_y\left(\frac{\partial\phi}{\partial y}\right)^2\right.\\ \left.-2\left(Q-c\rho\frac{\partial\phi}{\partial t}\right)\phi\right]\mathrm{d}V-\int_{S_1}\int\int q^*\phi\,\mathrm{d}S\\ +\frac{1}{2}\int_{S_2}\int h_c(\phi-\phi_\infty)^2\,\mathrm{d}S\end{aligned} \tag{32}$$

where h_c is the coefficient of convection, ϕ_∞ is the value of the field variable away from the boundary, V is the volume of the domain of interest (structure), S is its surface, S_1 and S_2 are portions of the boundary or surface over which potential flow q^*, and convection loss $h_c(\phi-\phi_\infty)$ are specified, respectively. Using customary finite element notation, Eq. (32) can be written in matrix form as

$$\begin{aligned}\pi_h=\frac{1}{2}\{a\}^T\int_V\int\int[[B]^T[D][B]]\,\mathrm{d}V\{a\}\\ -\{a\}^T\int_V\int\int[N]^TQ\,\mathrm{d}V\\ +\int_V\int\int\rho c[N]^T\{a\}^T[N]\frac{\partial\{a\}}{\partial t}\,\mathrm{d}V\\ -\{a\}^T\int_{S_1}\int[N]^Tq^*\,\mathrm{d}S\\ +\frac{1}{2}\int_{S_2}\int h_c\left[\left(\{a\}^T[N]^T[N]\{a\}\right.\right.\\ \left.\left.-(\{a\}^T[N]^T+[N]\{a\})\phi_\infty+\phi_\infty^2\right)\right]\mathrm{d}S\end{aligned} \tag{33}$$

where $\{a\}$ is the vector representing the nodal values of the field variable, $[N]$ is the shape function matrix, $[D]$ is the material property matrix and

$$[B]=\begin{bmatrix}\frac{\partial N_i}{\partial x} & \frac{\partial N_j}{\partial x} & \frac{\partial N_m}{\partial x}\\ \frac{\partial N_i}{\partial y} & \frac{\partial N_j}{\partial y} & \frac{\partial N_m}{\partial y}\end{bmatrix} \tag{34}$$

Using the principle of stationary potential, we take the derivative of Eq. (33) with respect to the nodal variables, to obtain

$$\begin{aligned}\frac{\partial\pi_h}{\partial\{a\}}=\int_V\int\int\left[[B]^T[D][B]\right]\mathrm{d}V\{a\}\\ -\int_V\int\int[N]^TQ\,\mathrm{d}V\\ +\frac{\partial\{a\}}{\partial t}\int_V\int\int\rho c[N]^T[N]\,\mathrm{d}V\\ -\int_{S_1}\int[N]^Tq^*\,\mathrm{d}S+\int_{S_2}\int h[N]^T[N]\{a\}\,\mathrm{d}S\\ -\int_{S_2}\int h[N]^T\phi_\infty\,\mathrm{d}S=0\end{aligned} \tag{35}$$

Using the previous definitions for the transfer and force matrices, we obtain the element equations as:

$$[k]\{a\}+[m]\{\dot{a}\}=\{f\} \tag{36}$$

where the superscript dot denotes differentiation with respect to time,

$$[k]=\left[\int_V\int\int\left[[B]^T[D][B]\right]\mathrm{d}V+\int_{S_2}\int h[N]^T[N]\,\mathrm{d}S\right] \tag{37}$$

and

$$[m]=\int_V\int\int c\rho[N]^T[N]\,\mathrm{d}V \tag{38}$$

$$\begin{aligned}\{f\}=\int_V\int\int[N]^TQ\,\mathrm{d}V+\int_{S_1}\int[N]^Tq^*\,\mathrm{d}S\\ +\int_{S_2}\int[N]^Th_c\phi_\infty\,\mathrm{d}S\end{aligned} \tag{39}$$

In Eqs. (37)–(39), the integrations are performed over the volume of each finite element. The global balance equations can be set-up by assembling the element balance equations in accordance with customary finite element techniques and can be represented as

$$[K]\{A\}+[M]\{\dot{A}\}=\{F\} \tag{40}$$

where $[K]$ is the global conduction matrix, $\{A\}$ is the global vector of nodal unknowns, $[M]$ and $\{F\}$ are the global counterparts of $\{m\}$ and $\{f\}$ in Eqs. (38) and (39), respectively.

The solution of the Eq. (40) is carried out using the following numerical time integration schemes [26]:

$$\begin{aligned}(\mathbf{M}+\mathbf{K}\beta\Delta t)A_{i+1}=[\mathbf{M}-\mathbf{K}(1-\beta)\Delta t]\mathbf{A_i}\\ +[(1-\beta)\mathbf{F_i}+\beta\mathbf{F_{i+1}}]\Delta t\end{aligned} \tag{41}$$

where β is a parameter which is chosen by the user, depending on the method of integration, Δt is the

selected time increment, and the bold symbols denote vectors and matrices.

Eq. (41) provides the time-marching scheme to solve for A_{i+1} using a time step Δt, and knowing the initial conditions $\mathbf{A_i}$ at the beginning of the time step. Any standard method of solution for simultaneous algebraic equations can be employed to solve the system of equations represented by Eq. (41).

It has been shown [26] that depending on the value of β, the time step may have an upper limit for the numerical integration to be stable. If $\beta < 0.5$, the largest value of Δt can be

$$\Delta t = \frac{2}{(1-2\beta)\lambda_{\max}} \tag{42}$$

where $\lambda_{\max}$ is the largest eigenvalue of

$$(\mathbf{K} - \lambda\mathbf{M})\mathbf{A}' = 0 \tag{43}$$

where $\mathbf{A}'$ representing the natural modes.

For $\beta \geqslant 0.5$, the solution is unconditionally stable. It has to be noted that this does not mean that the accuracy of the solution is guaranteed. If $\beta = 0$, the method is called "Forward Difference" or "Euler Method" while when $\beta = 0.5$, it is referred to as "Crank-Nicolson" or "Trapezoid" Rule. When $\beta = 3/2$ or 1, the methods are unconditionally stable and are called the "Galerkin's" and the "Backward Difference" methods, respectively. It has to be noted that methods which provide unconditional stability are used as a part of the prescribed algorithm. However, it is recognized that stability of the solution algorithm is guaranteed within the framework of a linear analyses. More information on numerical time integration schemes can be found in Zienkiewicz and Taylor [27,28].

8. Experimental verification

Experimental studies have been carried out by different researchers to investigate the carbonation problem in concrete structures [10,29–31]. Unfortunately, full data for the experiments (e.g. cement type, w/c, a/c, exposure conditions, etc.) have not been provided in every case. As a result, only the experiments conduced by Papadakis et al. [10] and in CEN Report-CR12793 [29] are used for the verification of the finite element model outlined in Figs. 2–5. First, a broad outline of the experimental work is described, followed by the finite element modeling of the test specimens.

8.1. Papadakis et al. tests

Papadakis et al. [10] conducted a series of accelerated carbonation tests. In this study, eight different $100 \times 100 \times 300$-mm concrete prisms were tested. After 90 days of moist curing at 30 °C, the specimens were oven-dried

Table 1
The exposure conditions for the specimens tested

Experiment	Specimen #	CO_2 (%)	RH (%)	T (°C)	Exposure
Papadakis et al. [10]	1	50	65	30	1, 3, 5, 10, 15, 20 days
	2	50	65	30	1, 3, 5, 10, 15, 20 days
	3	50	65	30	1, 3, 5, 10, 15, 20 days
	4	50	65	30	1, 3, 5, 10, 15, 20 days
	5	50	65	30	1, 3, 5, 10, 15, 20 days
	6	50	65	30	1, 3, 5, 10, 15, 20 days
	7	50	65	30	1, 3, 5, 10, 15, 20 days
	8	50	65	30	1, 3, 5, 10, 15, 20 days
	9	50	35	30	5 days
	10	50	45	30	5 days
	11	50	55	30	5 days
	12	50	65	30	5 days
	13	50	70	30	5 days
	14	50	85	30	5 days
	15	50	65	22	5 days
	16	50	65	30	5 days
	17	50	65	42	5 days
CEN Report [29]	1	0.035	70	22	1 year
	2	0.035	65	20	
	3	0.035	65	20	
	4	0.035	70	20	
	5	0.035	65	20	
	6	0.035	50	20	
	7	0.035	55	20	

and all surfaces were covered with a gas-tight paint except for two opposite surfaces, each with 100 × 300 mm dimensions.

The specimens were placed in a control chamber and exposed to a continuous flow of air with 50% CO_2. The temperature and relative humidity of the chamber were controlled during the experiment. Carbonation depth measurements for the specimens were taken at 1, 3, 5, 10, 15 and 20 days under various temperature (22, 30 and 42 °C) and relative humidity (35%, 45%, 55%, 65%, 70% and 85%) conditions.

8.2. Experimental data from CEN report: CR 12793 (1997)

The experimental study conducted by the authors of the CEN test method for the measurement of the carbonation depth of hardened concrete was presented by Jones et al. [29]. In this study, 100 × 100 × 400-mm concrete prisms were tested for carbonation. All of the

Table 2
Input parameters used in the finite element modeling one-dimensional tests [38–40]

Parameter	Value
Specific heat	1000 J/kg °C
Coefficient of conduction	2 W/m °C
Density of concrete	2400 kg/m^3
Adsorption isotherm	BET
Carbonation decay	Bi-linear: $a = 0.5$, $b = 90$

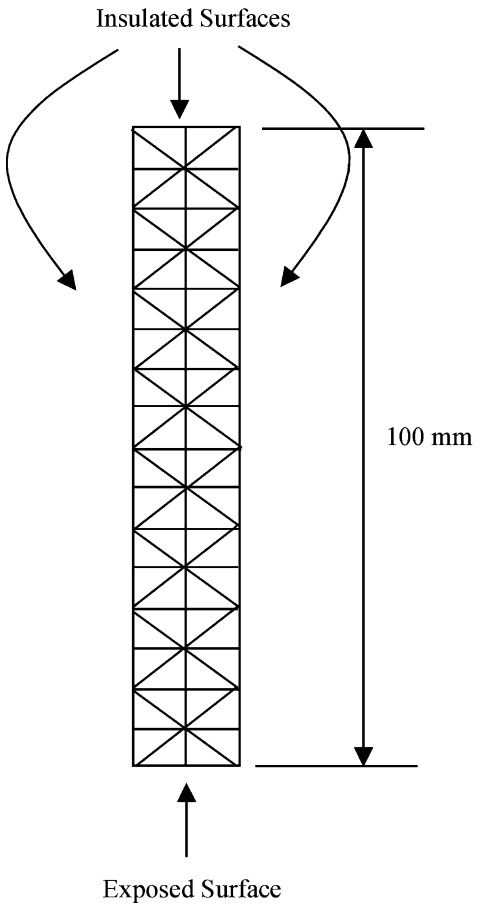

Fig. 6. The finite element mesh used to model the one-dimensional CO_2 ingress.

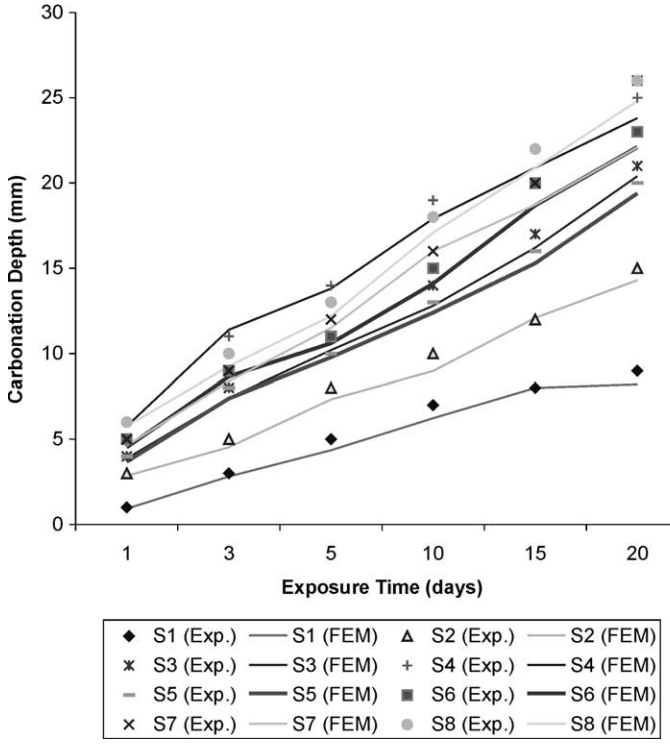

Fig. 7. Comparison of the results of Papadakis et al. [10] with CONDUR (specimens: 1–8).

specimens were cured under hessian and impermeable plastic sheeting for 24 h and for three days uncovered in the mould. The test specimens were exposed to 0.035% CO_2, 55–70% relative humidity and 22 °C temperature for one year. Carbonation readings were taken at 29, 91, 182, 273 and 364 days. The carbonation depth in each of the foregoing experimental studies was identified by spraying phenolphthalein on the sliced surfaces of the specimens.

8.3. Finite element analysis

A summary of the exposure conditions of all three groups of tests is provided in Table 1. The input data, including material properties, used in the analysis are given in Table 2. BET adsorption isotherm was used to relate the evaporable water content with the water vapour content. A bi-linear carbon dioxide decay function with $a = 0.6$ and $b = 90$ was used to simulate the change in porosity due to carbonation. The mineralogical characteristics of a typical OPC; i.e. C_3S: 55%, C_2S: 20%, C_3A: 12%, C_4AF: 13%, was used to model the composition of cement in the analyses.

The finite element mesh in Fig. 6, which is composed of 160 triangular elements, was used for the analysis of these one-dimensional carbonation problems. Only the nodes along the bottom edge of the mesh was exposed to the carbon dioxide while the other edges were assumed

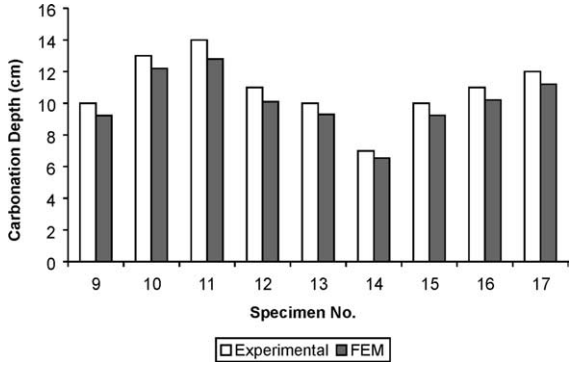

Fig. 8. Comparison of the results of Papadakis et al. [10] with CONDUR (specimens: 9–17).

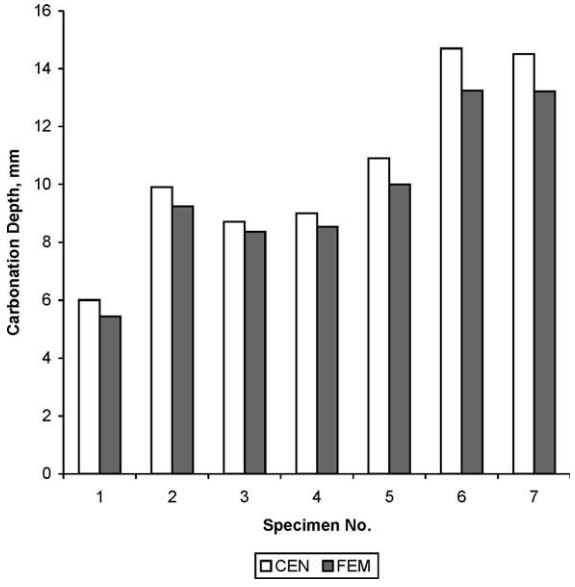

Fig. 9. Comparison of CEN data [29] with results of proposed FEM analysis after one year of exposure.

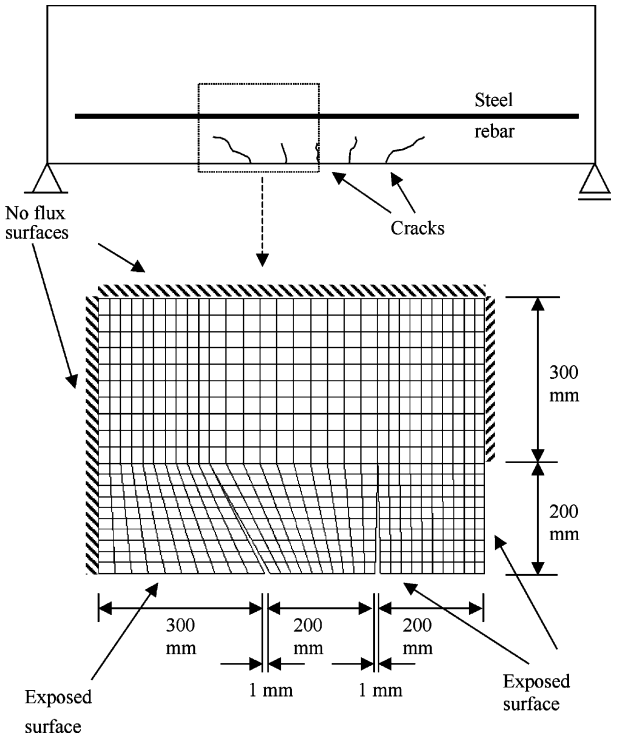

Fig. 10. Finite element modeling of a cracked beam for coupled heat, moisture, CO_2 transfer and carbonation analysis.

Table 3
Exposure conditions along the exposed surfaces of the numerical example

Months	T (°C)	RH (%)	CO_2 (%)
January	−10	55	0.3
February	−4	60	0.25
March	1	65	0.2
April	4	70	0.15
May	12	75	0.1
June	21	80	0.1
July	25	85	0.1
August	27	90	0.15
September	18	85	0.2
October	11	75	0.25
November	2	70	0.25
December	−4	65	0.3

to be insulated. Analysis for Papadakis et al. tests was carried out for 30 days with 1-h time increments. The analyses for the tests in the CEN report were carried out for one year with 1-day time increments.

Figs. 7–9 illustrate the carbonation depth advance versus time for the various test specimens as measured experimentally and as obtained from FEM analysis. The largest difference in the experimental and calculated results is 14%. The finite element model results are in close agreement with the carbonation measurements reported in the referred literature.

9. Numerical example

Due to the one-dimensional flow condition and the essentially non-variable exposure conditions of the previous tests, the capability of the proposed finite element model cannot be fully gauged by the analyses in the previous section. The presented model can be used to solve two-dimensional problems with variable boundary and exposure conditions and to investigate the influence of discrete cracks on heat, moisture and CO_2 transfer processes as well as on carbonation reactions. It also

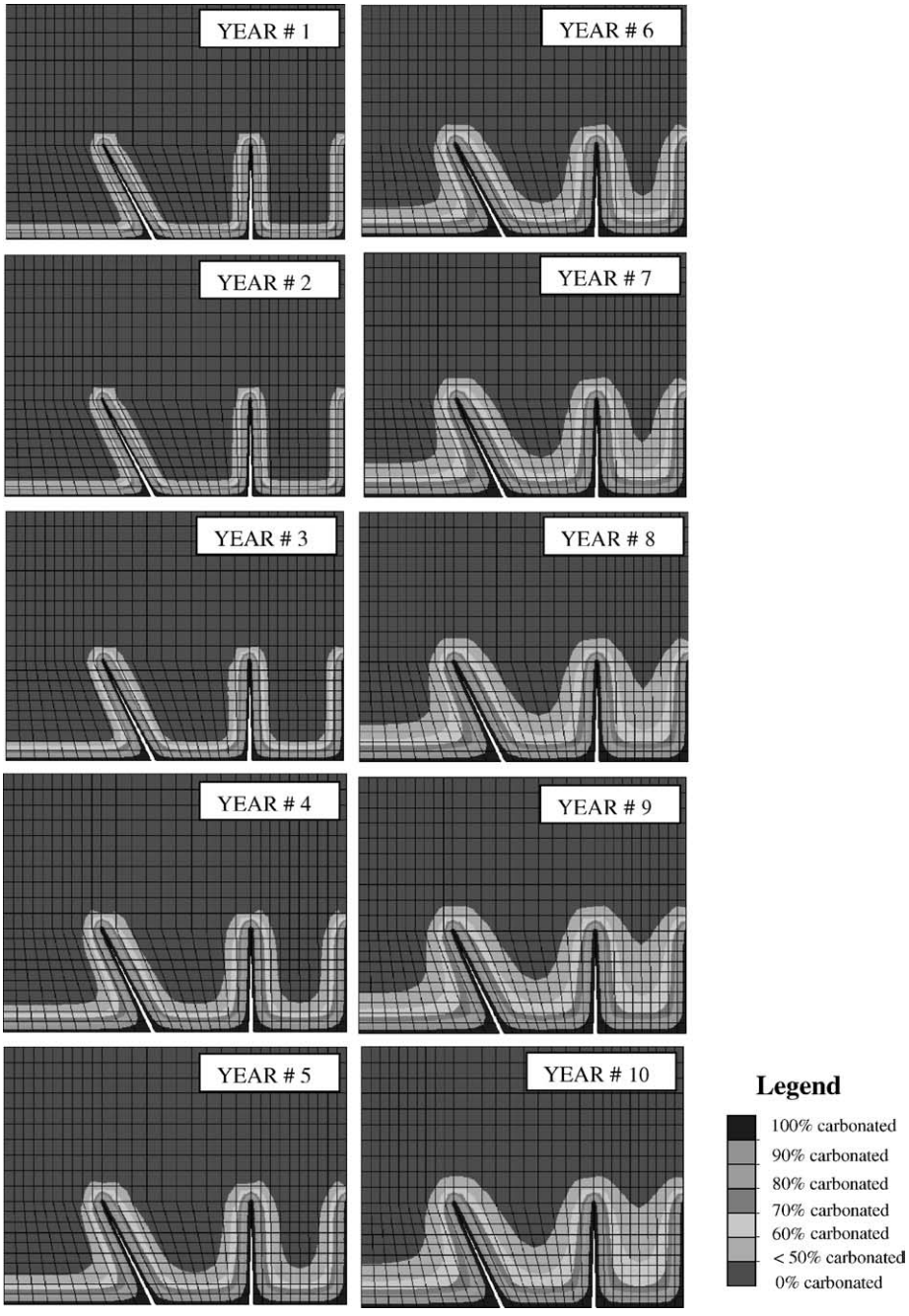

Fig. 11. Annual carbonation front over a 10-year period.

permits one to consider high exposure regions, variable concrete properties in the same structure, and the effect of overlays and repaired concrete on carbonation.

It should be mentioned that in modeling the transport properties of local cracks, discrete or distributed, permeability is affected by many factors, including cracks opening, tortuosity, distribution, orientation and connectivity, phenomena which require further research. In finite element models, the effect of highly distributed cracks can be accounted for through empirical transport coefficients. Discrete cracks, larger than a predefined size, can be treated as gaps within the finite element mesh and the crack faces can be treated as free surfaces, a procedure adopted in the current study and one which cannot be handled by a one-dimensional analysis. The writers are cognizant that more experimental and analytical studies are needed to fully understand the effect of crack parameters on transport properties of concrete.

In order to simulate a real-life structure, the example in Fig. 10 is solved by using the developed computer program. The beam is assumed to be cracked, with crack depth being 20 mm and maximum crack width being 1.0 mm at the surface. The composition of cement used in the beam, whose specific gravity and fineness, respectively, are 3.15 and 300 m^2/kg, is given in Table 2. The water–cement ratio (w/c) and aggregate–cement ratio (a/c) of the initial mix are assumed to be 0.49 and 3, respectively. The average specific gravity of the aggregates is assumed to be 2.6. Initially, the concrete is assumed to have 65% relative humidity and 0% CO_2. The monthly temperature, relative humidity and CO_2 profiles during one year of exposure are given in Table 3.

The analysis is started in May and continued for 10 years. The movement of the carbonation front over 10 years is illustrated in Fig. 9. It should be noted that the results are reported in terms of "% carbonated" which gives the percentage of initial $Ca(OH)_2$ consumed. For example, a 60% carbonated means that 40% of the initial $Ca(OH)_2$ content is still available to react with CO_2.

The proposed model shows that the ambient temperature and moisture changes in the environment have a direct effect on CO_2 diffusion and carbonation of concrete. For example, at −10 °C temperature and 55% relative humidity, the carbon dioxide diffusion coefficient in concrete at a specific location in the structure, calculated after one year of exposure, was 1.56×10^{-10} m^2/s; while at the same location and time, at 27 °C and 90% relative humidity, it was calculated to be 5.71×10^{-8} m^2/s, or nearly 400 times larger.

Fig. 11 shows the carbonation depth within the member for 10 years of exposure. It is important to notice the effect of relatively wide discrete cracks on the carbonation of the concrete beam. An analysis without considering the cracks would not simulate the situation accurately nor would a one-dimensional analysis scheme because the orientation of the cracks and the variable exposure conditions require a two-dimensional solution. This can be observed better in Fig. 12 in which a comparison is made between results of a one-dimensional versus a two-dimensional analysis. The difference in carbonation depth between the two cases underlines the importance of the cracks and of their proper modeling in carbonation analyses. Unfortunately, due to lack of experimental data, the two-dimensional analyses cannot be verified.

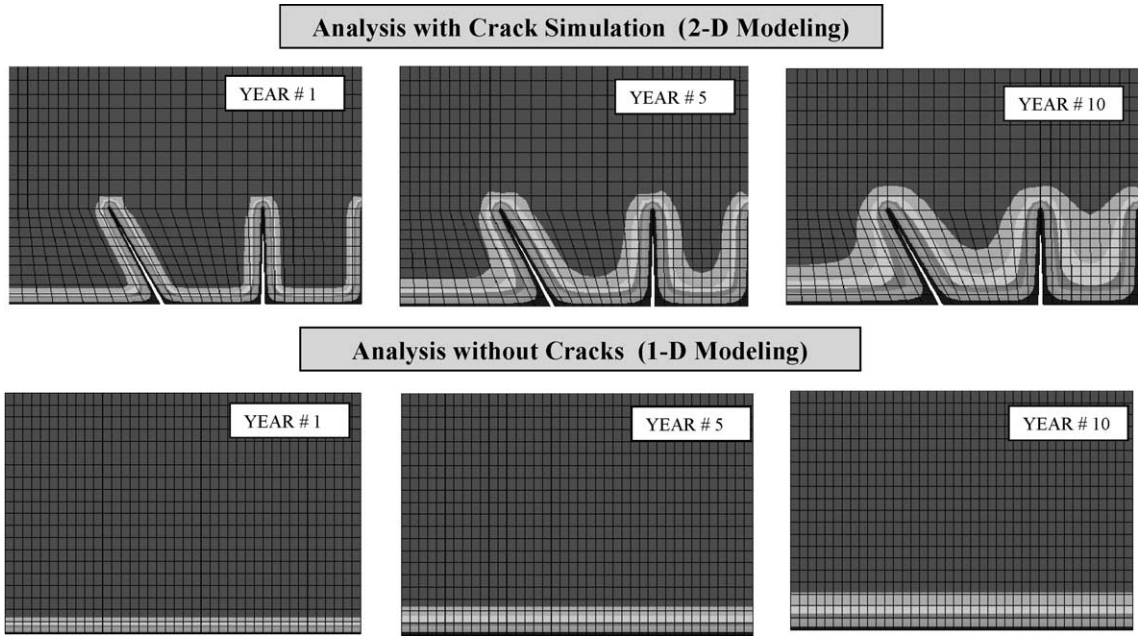

Fig. 12. Effect of the presence of cracks on the carbonation of concrete.

10. Summary and conclusions

A systematic and robust method for predicting carbonation in concrete structures under prescribed exposure conditions is developed. The significant phenomena that contribute to the rate and amount of carbonation; i.e. heat and moisture transfer and CO_2 transport are modeled by the two-dimensional time-dependent nonlinear finite element method. The governing equations of the various transport phenomena are solved numerically in the time and the space domains. Where appropriate, the coupling effects among the different transport phenomena and the carbonation process are modeled in order to simulate the field conditions reasonably closely. The proposed finite element model and its associated computer program, CONDUR, are capable of handling any geometry (including cracks), prescribed initial and boundary conditions and pertinent material nonlinearities.

Comparison with one-dimensional experimental data, in the absence of two-dimensional experimental studies, show that the proposed model can predict the carbonation process quite accurately. The following conclusions can be reached from the numerical solutions based on the proposed model:

1. The modeling of carbonation in concrete is a complex problem which requires, for realistic simulation, a systematic and robust finite element approach in the time and the two-dimensional space domain. The approach adopted here is able to handle the coupling effects and material nonlinearities, which are inherent to reinforced concrete durability problems, and is capable of closely modelling different geometries, initial and boundary conditions.
2. The results of the proposed method of analysis agree well with available experimental data from one-dimensional CO_2 diffusion tests.
3. One-dimensional models, which are widely used to investigate CO_2 penetration into concrete, have limited applicability because they are unable to capture the effects of imperfections and variabilities in concrete properties or local exposure conditions.
4. The presence of cracks has an important effect on the transport properties of concrete, including carbon dioxide diffusion. Since it is almost impossible to find concrete structures without cracks, reinforced concrete durability models should have the capability to simulate cracks. The finite element method can easily model discrete cracks, while smeared or micro-cracks can be accounted for via the material transport properties. However, further studies are needed to define mass transport properties of cracks.
5. The available models for carbonation, although primarily developed based on test data simulating one-dimensional flow, can be extended via the finite element technique to two-dimensional transport conditions. However, suitable experimental data from two-dimensional diffusion tests are needed to verify the accuracy of the finite element results.

Acknowledgements

This research was supported by a grant from the Natural Sciences and Engineering Research Council (NSERC) of Canada, which is gratefully acknowledged.

References

[1] Verbeck GJ. Mechanisms of corrosion in concrete. Corrosion of metals in concrete, SP-49, ACI, 1975. p. 21–38.
[2] Parrott LJ. Carbonation, moisture, and empty pores. Adv Cement Res 1991;4(15):111–8.
[3] Currie RJ. Carbonation depths in structural quality concrete. Building Research Establishment Report Watford, UK, 1986. 19pp.
[4] Ho DWS, Lewis RK. Carbonation of concrete and its prediction. Cement Concr Res 1987;17:489–504.
[5] Wierig HJ. Longtime studies on the carbonation of concrete under normal outdoor exposure. RILEM Symposium on Durability of Concrete under Normal Outdoor Exposure, Hanover, Germany, 1984. p. 192–6.
[6] ACI Committee 201, Guide to Durable Concrete (ACI 201.2R-92) (Reapproved 1997).
[7] CAN/CSA-A23.1/A23.2-00, Concrete Materials and Methods of Concrete Construction/Methods of Test for Concrete, 2000.
[8] Neville A. Properties of concrete. fourth ed New York, USA: John Wiley and Sons Inc; 1996.
[9] Johannesson BF. Non-linear transient phenomena in porous media with special regard to concrete durability. Adv Cement Based Mater 1997;6:71–5.
[10] Papadakis V, Vayenas CG, Fardis MN. Fundamental modeling and experimental investigation of concrete carbonation. ACI Mater J 1991;88(4):363–73.
[11] Johannesson BF. Modeling of transport processes involved in service life prediction of concrete: important principles. Licentiate Thesis, Lunds University, Sweden, 1998. 227pp.
[12] Beaudoin J. Private communication, 2001.
[13] Saetta A, Schrefler B, Vitalini R. The carbonation of concrete and the mechanism of moisture, heat, carbon dioxide flow through porous materials. Cement Concr Res 1993;23(4):761–72.
[14] Sickert G. Extended modeling for the advance of carbonation in concrete. Concr Precasting Plant Technol 1997;12:74–88.
[15] Emerson M. The Calculation of the Distribution of Temperature in Bridges. TRRL Report LR561, Department of the Environment, Crowtowne, England, 1973.
[16] Priestley MJN. Linear heat-flow analysis of concrete bridge decks. Research Reports 76/3, Department of Civil Engineering, University of Canterbury, Christchurch, 1976.
[17] Therkeld JL. Thermal environmental engineering. second ed. Prentice-Halll; 1970.
[18] Clausing AM. Basic definitions and formulas. Class Notes in Solar Engineering, University of Illinois, Urbana, IL, 1976.
[19] Priestley MJN, Thurston S. Discussion of the Paper Titled "Thermal Calculations for Bridge Design" by Hunt et al. ASCE J Struct Div, 1979;102(ST6):1277–9.

[20] Potgieter IC, Gamble W. Response of Highway Bridges to Nonlinear Temperature Distributions. Structural Engineering Series No. 505, Report No. FHWA/IL/UI-201, 1983. 291pp.
[21] Martín-Pérez B. Service Life Modeling of R.C. Highway Structures Exposed to Chlorides. Ph.D. Thesis, University of Toronto, Canada, 1999. 168pp.
[22] Xi Y, Bazant ZB, Jennings HM. Moisture diffusion in cementitious materials: Adsorption isotherm. J Adv Cement Based Mater 1994;1:248.
[23] Martys NS. Diffusion in partially saturated porous materials. Mater Struct 1999;32:555–62.
[24] Isgor OB. A Durability Model for Chloride and Carbonation Induced Steel Corrosion in Reinforced Concrete Members. Ph.D. Dissertation, Carleton University, Ottawa, Ontario, Canada, 2001. 268pp.
[25] Logan DL. A first course in finite element method. Boston: PWS Publishing; 1992. 617 pp.
[26] Hughes TJR. The finite element method—linear static and dynamic finite element analysis. New York: Dover Publishers; 2000.
[27] Zienkiewicz OC, Taylor RL. The finite element method, 1: basic formulation and linear problems. fourth ed. McGraw Hill; 1989. 648pp.
[28] Zienkiewicz OC, Taylor RL. The finite element method, 2: solids and fluid mechanics, dynamics and non-linearity. fourth ed. McGraw Hill; 1991. 648pp.
[29] Jones MR, Dhir RK, Newlands MD, Abbas AMO. A study of the CEN test method for measurement of the carbonation depth of hardened concrete. Mater Struct 2000;3:135–42.
[30] Ho DWS, Lewis RK. Carbonation of concrete and its prediction. Cement Concr Res 1987;17:489–504.
[31] Schutter GDe. Quantification of the influence of cracks in concrete in concrete structures on carbonation and chloride penetration. Mag Concr Res 1999;51(6):427–35.